

Cite this: DOI: 00.0000/xxxxxxxxxx

Numerical insights on the volume phase transition of thermoresponsive hollow microgels[†]

Leah Rank^{a,b} and Emanuela Zaccarelli^{*a,b}Received Date
Accepted Date

DOI: 00.0000/xxxxxxxxxx

Hollow microgels, consisting of a pNIPAM polymer network with a central cavity, have significant potential due to their tunable softness and encapsulation capabilities. Using molecular dynamics simulations, we thoroughly characterise the swelling behaviour of neutral hollow microgels across the Volume Phase Transition (VPT) upon varying crosslinker concentration, shell thickness, and size. In particular, we examine in detail the onset of cavity filling and its relation to the VPT, detecting the presence of a discontinuity in the radius of gyration of the microgels, if an appropriate balance between shell stiffness and thermoresponsiveness is reached. The discontinuity is, however, absent in the behaviour of the hydrodynamic radius, in agreement with experimental observations. We then test our numerical model by direct comparison of form factors with available measurements in the literature and also establish a minimal-size, stable hollow microgel for future computationally feasible bulk investigations. Overall, our findings provide valuable insights into the fundamental swelling properties of hollow microgels that can be useful to control the opening and closing of the cavity for application purposes.

1 Introduction

Microgels are synthetic polymer networks¹, typically ranging from a few tenths of nanometers up to a few microns in size. Depending on the constituent polymers, they display reversible swelling properties in response to environmental changes, *e.g.*, temperature^{2–4}, pH^{5,6} or salt concentration^{7,8}. In particular, thermoresponsive microgels undergo a so-called volume phase transition (VPT), shifting from a swollen to a collapsed state at a specific temperature. This transition reflects the underlying coil-to-globule transformation of the polymer chains, induced by worsening solvent conditions as the temperature increases⁹. Microgels made of Poly-N-isopropylacrylamide (pNIPAM) are among the most studied ones, with the VPT occurring at around 32°C¹⁰. The combination of softness and responsiveness makes them ideal systems for fundamental condensed matter research^{11–13} and for numerous applications in material science

that exploit their controllable bulk behaviour^{14–17}.

Among the different topologies, hollow microgels, *i.e.*, polymer network shells with an internal cavity, stand out as particularly intriguing. Even more than their non-hollow counterparts, these structures hold great potential as carriers encapsulating smaller nanoparticles, such as drugs, that require controlled release to specific areas in the body^{18–20}. Furthermore, hollow microgels are of fundamental interest for their similarities to vesicles and cells²¹, due to their unique elastic properties allowing them to mimic the mechanical behaviour of these biological systems. Notably, the buckling of hollow microgels has been observed under specific osmotic conditions²². This phenomenon involves a shape transformation where the initially spherical microgel structure collapses asymmetrically, forming a double-layered, bowl-like morphology. Driven by osmotic pressure gradients, this transition results in a concave configuration with a distinctive inward folding that imparts a characteristic double-walled structure to the microgel^{20,22}. This is analogous to what has been seen in soft vesicles²³ and red blood cells²⁴, where soft particles deform under certain mechanical stresses.

However, to ensure efficient applications, it is important to tune the cavity size relative to the shell thickness and to understand how this ratio influences the behaviour as a function of temperature. In this context, Dubbert *et al.*¹⁸ explored different experimental conditions to monitor the cavity's stability, even above the VPT temperature (VPTT). They found that preserving and stabilising the hollow structure comes at the expense of ef-

^a CNR Institute of Complex Systems, Uos Sapienza, Piazzale Aldo Moro 2, 00185, Roma, Italy

^b Department of Physics, Sapienza University of Rome, Piazzale Aldo Moro 2, 00185 Roma, Italy; Email: emanuela.zaccarelli@cnr.it

[†] Electronic Supplementary Information (ESI) available: [details of any supplementary information available should be included here]. See DOI: 10.1039/cXsm00000x/

‡ Additional footnotes to the title and authors can be included *e.g.* 'Present address:' or 'These authors contributed equally to this work' as above using the symbols: ‡, §, and ¶. Please place the appropriate symbol next to the author's name and include a `&footnotetext` entry in the the correct place in the list.

efficient thermo-responsive behaviour. Another control parameter for the rigidity is the crosslinker concentration within the shell, which has been studied by the formerly mentioned work as well as Contreras-Cáceres et al.²⁵ who used various microscopy techniques to identify the microgel's shape in detail. As expected, these authors found that increasing the crosslinker concentration helps to maintain the cavity open at high temperatures, causing the microgel to be less responsive to temperature increase. The aim to further examine hollow microgels and their swelling behavior is therefore to be able to tune their stiffness such that they maintain their hollowness up to the desired temperatures, but still responding to temperature variation in terms of shrinking. For some specific purposes it may be also useful to tune the occurrence of the filling of the cavity below or above the VPT temperature. Most of the available experimental studies of hollow microgels are based on the use of a degradable core on which a Poly(N-isopropylacrylamide) (pNIPAM) shell is built.^{18,20,25–27} This method allows for producing almost monodisperse hollow microgels. Other studies have employed an alternative protocol, where the microgel shell is synthesised around an inner microgel, rather than a solid core, which is also subsequently dissolved^{28,29}. Comparisons of the hollow microgels obtained this way with numerical simulations²⁹ indicate that the resulting shell is significantly less dense in monomers than standard microgels, likely due to the complex interplay between the two networks. In contrast, an extensive numerical characterisation of hollow microgels synthesised around a solid core, particularly regarding their behaviour across the VPT, and a detailed comparison to experiments, are still lacking.

The present study aims to fill this gap by examining the single-particle properties of neutral hollow microgels with varying shell thicknesses, total sizes, and crosslinker concentrations to be able to obtain tunable hollowness with added thermo-responsive character using the right balance of the synthesis parameters. We test our numerical model by comparing the numerical form factors with available experimental ones for both very large microgels²⁰ and for more standard ones¹⁸, measured respectively by Static Light Scattering and by Small Angle Neutron scattering, for two different temperatures above and below the VPT. Additionally, we also assess size effects to stabilise the inner cavity of the hollow microgels while using a minimal number of monomers, paving the way for future computationally feasible investigations of their collective behaviour. The main findings of our study are devoted to unveiling the complex interplay between the occurrence of the VPT, influenced by solvent-polymer interactions, and the closing of the cavity, which needs to overcome the elastic response of the network, as a function of the various synthesis parameters mentioned above. We present evidence of specific conditions — namely, a high crosslinker concentration combined with a moderate shell thickness — under which the size of the microgel, expressed by the radius of gyration, exhibits a peculiar discontinuity as a function of temperature, signaling the filling of the cavity. Varying the combinations of parameters, we find situation where the hole disappears even before the VPTT or it does not close at all up to extremely elevated temperatures, well beyond those studied in the experiments. Our results are rationalized in the

context of existing experimental findings^{18,20,25}, thereby offering a useful map of the different parameter combinations that can be employed to achieve the preservation of the hollowness up to the desired temperatures.

2 Model and Methods

2.1 Assembly

Our numerical protocol to assemble disordered polymer networks is based on previous works³⁰ exploiting the oxDNA simulation package³¹. Specifically, we use a binary mixture of patchy particles, representing monomers as bivalent particles and crosslinkers as tetravalent ones. All the particles have mass m_m and diameter σ_m , which serve as the units of mass and length, respectively. During the Molecular Dynamics (MD) simulations of the assembling process, all particles are confined within a sphere using a stiff harmonic potential acting at radius Z_{out} . The molar concentration of the crosslinkers c is varied between 1% and 10% according to most common experimental values.

To make the microgels hollow, all particles are also prevented from entering an inner spherical region²⁹ via a gravitational force acting symmetrical around the center of the outside barrier, with radius $Z_{\text{in}} < Z_{\text{out}}$, as illustrated in Figure 1 (a). After almost all of the bonds ($\gtrsim 99.8\%$) are formed, most of the particles are found in one big cluster and the remaining particles not belonging to the big network (consisting of $N_m = \rho_m \cdot (4\pi/3)(Z_{\text{out}}^3 - Z_{\text{in}}^3)$ monomers) are removed.

The total number of particles N_m is chosen to achieve the number density $\rho_m \approx 0.08$, as established by successful comparison to experiments for standard microgels^{20,32}. We note that in Ref.²⁹, the number density used for hollow microgels synthesised around an inner microgel is approximately $\rho_m \approx 0.03$, significantly lower than in our current study due to interpenetration with the inner network. Here, the solid inner core does not extend into the shell region, therefore we maintain the density consistent with standard microgels. While standard microgels require an additional force on the more reactive crosslinkers to sustain the core-corona structure, we assume that this additional force can be neglected here, given the reduced assembly volume of the shell.

2.2 Alternative assembly in the presence of a core

In an attempt to better stabilise the cavity with a low number of monomers, we also tested an alternative assembly approach, inspired by the experimental synthesis. To this aim, we place a fixed core of radius Z_{in} in the middle of the assembly volume, which physically prevents particles from entering, thus creating the nominal cavity of the hollow microgel, as shown in Fig. 1 (b). For simplicity, the core is made up of a tight single layer of immobile particles, which only interact with the rest of the patchy particles via excluded volume interactions. For simplicity, no bonds between the core and the monomers or crosslinkers are formed. After the assembly is completed, with $\gtrsim 99.8\%$ bonds formed as for standard microgels, we still retain only the biggest cluster for subsequent analysis and the inner core is removed.

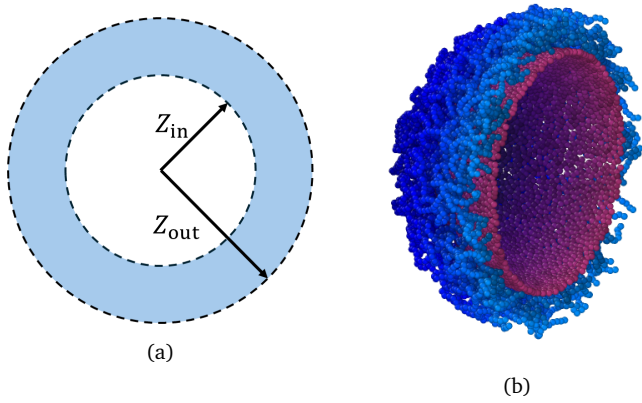


Fig. 1 Sketch of the assembly process illustrating: (a) particles confined within a shell of outer radius Z_{out} and inner radius Z_{in} ; (b) a hollow shell (blue monomers) assembled around an immobile physical core (magenta particles).

2.3 Microgel simulations

Independently of the employed assembly method, once the network is formed, the attractive patches are replaced by permanent bonds³⁰, represented by the well-known bead-spring model of Kremer and Grest³³. In particular, non-bonded monomers experience an excluded volume interaction, modeled as a Weeks-Chandler-Andersen (WCA) potential,

$$V_{\text{WCA}}(r) = \begin{cases} 4\epsilon \left(\left(\frac{\sigma_m}{r} \right)^{12} - \left(\frac{\sigma_m}{r} \right)^6 \right) + \epsilon & \text{if } r \leq 2^{1/6} \sigma_m \\ 0 & \text{otherwise,} \end{cases} \quad (1)$$

while the bonded monomers additionally interact with the finite extensive nonlinear elastic (FENE) potential allowing for unbreakable bonds,

$$V_{\text{FENE}}(r) = -\epsilon k_{\text{F}} R_0^2 \ln \left(1 - \left(\frac{r}{R_0 \sigma_m} \right)^2 \right), \quad \text{if } r < R_0 \sigma_m. \quad (2)$$

The parameter ϵ defines our unit of energy, $k_{\text{F}} = 15$ is the spring constant and $R_0 = 1.5$ is the maximum bond extension. To model the effect of increasing temperature, we use a solvophobic potential^{34,35} that models the increasing repulsion to the solvent as an effective attraction between the monomers:

$$V_{\alpha}(r) = \begin{cases} -\epsilon \alpha & \text{if } r \leq 2^{1/6} \sigma_m \\ \frac{1}{2} \epsilon \alpha [\cos(\gamma(r/\sigma)^2 + \beta) - 1] & \text{if } 2^{1/6} \sigma_m < r \leq R_0 \sigma_m \\ 0 & \text{otherwise} \end{cases} \quad (3)$$

with $\beta = 2\pi - 2.25\gamma$, $\gamma = \pi/(2.25 - 2^{1/3})$. The parameter α acts as an effective temperature: for $\alpha = 0$ the microgel is in good solvent conditions, while the volume phase transition (VPT) occurs around $\alpha \approx 0.63$. MD simulations are conducted at a fixed temperature, $T^* = k_{\text{B}} T = 1.0$, where k_{B} is the Boltzmann constant. To ensure a constant temperature, the Nose-Hoover thermostat³⁶ is used, following a leapfrog integration scheme with a time step $\delta t^* = \delta t \sqrt{\epsilon/(m_{\text{m}} \sigma_m)} = 0.002$. The simulations have been conducted for each microgel individually, lasting up to 10^7 time steps.

We characterise the hollow microgels of various sizes using a

relative shell thickness, defined as $\delta_{\text{rel}} = (Z_{\text{out}} - Z_{\text{in}})/Z_{\text{out}}$. Further, we analyse the differences between the structure directly after assembly, where all particles lie between Z_{in} and Z_{out} , and the relaxed structure after equilibration, *i.e.*, evolution under the Kremer-Grest potential without boundaries, to determine how the microgel structure evolves depending on the initial assembly parameters.

2.4 Calculated observables

The swelling curve of a microgel is monitored by calculating its radius of gyration from equilibrated configurations, defined as

$$R_{\text{g}} = \left\langle \sqrt{\frac{1}{N_{\text{m}}} \sum_i (\vec{r}_i - \vec{r}_{\text{cm}})^2} \right\rangle, \quad (4)$$

where \vec{r}_i refers to the position of the i -th monomer and \vec{r}_{cm} to the microgel center of mass³⁷. The angled brackets denote an average over several configurations at different uncorrelated times of the equilibrated network. Alternatively, and more in line with experimental practices, the microgel size at different temperatures can be described by the evolution of the hydrodynamic radius R_{H} with temperature. Several definitions have been proposed in the recent past, but we calculate R_{H} following Refs.^{38,39}:

$$R_{\text{H}} = \left\langle 2 \left[\int_0^{\infty} \frac{1}{\sqrt{(a^2 + \theta)(b^2 + \theta)(c^2 + \theta)}} d\theta \right]^{-1} \right\rangle \quad (5)$$

where a, b, c are the principal semi-axes of the gyration tensor of the convex hull enclosing the microgel.

We also evaluate the radial density distribution $\rho(r)$ as a function of the distance $r = |\vec{r}|$ from the center of mass of the microgel, given by

$$\rho(r) = \left\langle \sum_{i=1}^{N_{\text{m}}} \delta(|\vec{r} - \vec{r}_i|) \right\rangle. \quad (6)$$

Finally, we calculate its representation in Fourier space, namely the form factor:

$$P(q) = \frac{1}{N_{\text{m}}} \left\langle \sum_{i,j} \exp(-i\vec{q} \cdot \vec{r}_{ij}) \right\rangle, \quad (7)$$

which is essential for comparison with experiments. The vector $\vec{r}_{ij} = \vec{r}_i - \vec{r}_j$ denotes the distance between monomer i and j within the microgel and the corresponding sum runs over all particle pairs.

2.5 Form Factor fits

To extract the density profiles from experimental data, it is necessary to perform adequate fits of the form factors. We can thus exploit simulations, where both quantities can be calculated directly, to evaluate the appropriateness of different fitting functions. Therefore, we first analyse the density profiles to identify a suitable functional form, which can then be converted via Fourier transformation to obtain a fitting function for the corresponding form factor. In order to provide a recipe to be followed also in experiments, we privilege the use of analytic functions for the density profiles containing significant parameters that sufficiently

describe the microgel's topology.

More specifically, we find that a suitable representation for the density profile of all simulated microgels is given by a parabolic description⁴⁰, which reads as

$$\rho_{\text{parab}}(r) = \begin{cases} \frac{a}{2} \frac{(r - (R_{\text{in}} - s_{\text{in}}))^2}{s_{\text{in}}^2} & \text{if } R_{\text{in}} - s_{\text{in}} < r \leq R_{\text{in}} \\ a - \frac{a}{2} \frac{(r - (R_{\text{in}} + s_{\text{in}}))^2}{s_{\text{in}}^2} & \text{if } R_{\text{in}} < r \leq R_{\text{in}} + s_{\text{in}} \\ a - \frac{a}{2} \frac{(r - (R_{\text{out}} - s_{\text{out}}))^2}{s_{\text{out}}^2} & \text{if } R_{\text{out}} - s_{\text{out}} < r \leq R_{\text{out}} \\ \frac{a}{2} \frac{(r - (R_{\text{out}} + s_{\text{out}}))^2}{s_{\text{out}}^2} & \text{if } R_{\text{out}} < r \leq R_{\text{out}} + s_{\text{out}} \\ 0 & \text{otherwise.} \end{cases} \quad (8)$$

This equation consists of four consecutive parabolas ($\rho_i(r)$ with $i = 1, 2, 3, 4$), schematically plotted in Figure 2 that visually explains the different defining parameters a , s_{in} , s_{out} , R_{out} , and $R_{\text{in}} = R_{\text{out}} - s_{\text{out}} - W$.

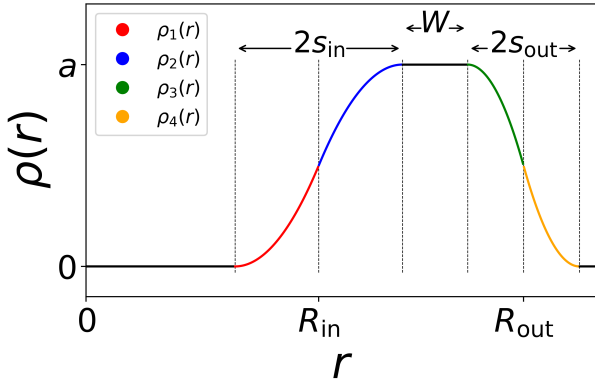


Fig. 2 Sketch of the density profile made up of four different consecutive parabolas, inspired by Ref.⁴⁰. From 0 to $R_{\text{in}} - s_{\text{in}}$, $\rho(r)$ is zero indicating the cavity region. The shell, roughly found between R_{in} and R_{out} , shows fading edges inward and outward analogously to the non-hollow microgel with a homogeneous core and a fuzzy corona.

To obtain the form factor, we first need to calculate the amplitude

$$A(q) = \int \rho_{\text{fit}}(r) e^{-iq \cdot \vec{r}} d\vec{r} \quad (9)$$

and hence each parabola can be analytically Fourier transformed to eventually get $A_{\text{parab}}(q) = A_{\text{parab}}(q, R_{\text{out}}, s_{\text{in}}, s_{\text{out}}, a)$, as detailed in the Appendix, giving a fitting function for $P(q)$:

$$P_{\text{parab}}(q) = \frac{A_{\text{parab}}(q)^2}{N_{\text{m}}^2} + \frac{I_0}{1 + \xi^2 q^2} \quad (10)$$

where a Lorentzian term with two extra fit parameters, the amplitude I_0 and the polymer network's average correlation length ξ , is added, as in experiments, to take into account the finite size of the microgel⁴¹. The normalisation is given by N_{m}^2 which is exactly known in simulations. The form factor can thus be fitted using all the fit parameters mentioned above that define the parabolic density profile as well as the two terms from the Lorentzian. Al-

ternatively, we can simply take the values from the fit parameters obtained from ρ_{parab} and fit only the Lorentzian part. As shown in the following, the results of the two approaches are virtually identical.

In addition, we notice that when we simulate small hollow microgels, the density profiles can be captured in two ways: either via the parabolic approach described above with $W = 0$ or via a Gaussian density profile of width σ :

$$\rho_{\text{gauss}}(r) = C \cdot \exp\left(-\frac{(r - \mu)^2}{2\sigma^2}\right). \quad (11)$$

Since this is a symmetric function, it requires even fewer fit parameters. Here, the form factor can be calculated with the formula put forward by Gradzielski et al.⁴², who have performed a calculation considering $\sigma < \mu$ that allows the lower integration limit to be $-\infty$. The resulting analytical Fourier transformation then leads to:

$$A_{\text{gauss}}(q) = C \cdot \frac{4\pi}{q} e^{(-q^2\sigma^2/2)} (\mu \sin(q\mu) + q\sigma^2 \cos(q\mu)) \quad (12)$$

Next, the amplitude $A_{\text{gauss}}(q)$ can be used in Eq. 10 the same way as for the parabolic case. To be more precise, for the smaller microgel in its hollow state, $W = 0$ is fixed, thus we have one less fit parameter, while $R_{\text{in}} = R_{\text{out}} - s_{\text{out}} - s_{\text{in}} - W = R_{\text{in}} = R_{\text{out}} - s_{\text{out}} - s_{\text{in}}$ can be calculated the same way as before, and the Gaussian mean value is approximately equivalent to $\mu = (R_{\text{out}} + R_{\text{in}})/2$, respectively $\sigma = (s_{\text{out}} + s_{\text{in}})/2$.

At high temperatures, when the microgels experience a collapse and the cavity vanishes, the above-mentioned fits no longer hold. In that case, we resort to the standard treatment of microgel structures in terms of the fuzzy sphere model³ which has been used in previous works³⁰ to describe density profiles of non-hollow microgels.

3 Results

3.1 Swelling behaviour of hollow microgels: a typical signature in the radius of gyration

Hollow microgels exhibit a similar deswelling behaviour upon temperature increase as their non-hollow counterparts, driven by the decreased solvating ability of the background liquid. However, due to their internal cavity, hollow microgels display an additional structural feature: the inner cavity collapses at elevated temperatures and low enough shell elasticity. We begin by demonstrating this unique swelling and collapse behaviour in a specific hollow microgel. For this purpose, we select the representative case where $\delta_{\text{rel}} = 0.275$ and $c = 5\%$. Snapshots at different temperatures are shown in Figure 3 (a) and the corresponding radial density distributions $\rho(r)$ are plotted in Figure 3 (b).

It is evident that up to $\alpha = 0.6$, just below the VPT, the microgel maintains its cavity intact, while eventually, for $\alpha = 0.8$ it has collapsed completely, filling up the initial hole, thus giving rise to a homogeneous profile along the inner part of the microgel. To be more quantitative, we perform simulations at many different values of α , finding that the hole fills at $\alpha_{\text{fill}} \approx 0.71$. This value is higher than the temperature of the VPT at $\alpha_{\text{VPT}} \approx 0.63$. We

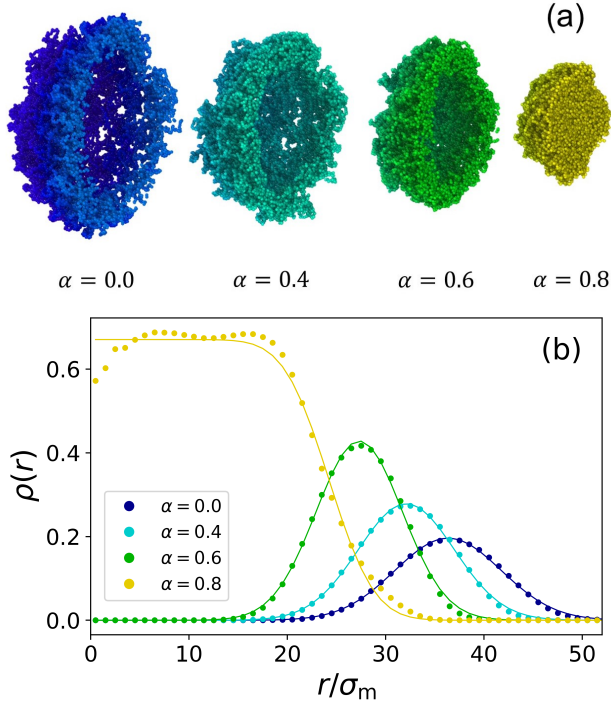


Fig. 3 (a) Snapshots of a hollow microgel with crosslinker percentage $c = 5\%$ and $\delta_{\text{rel}} = 0.275$ obtained from the assembly with $Z_{\text{out}} = 60\sigma_m$ and $Z_{\text{in}} = 43.5\sigma_m$ ($N_m \approx 44000$), at different effective temperatures: $\alpha = 0, 0.4, 0.6, 0.8$ from left to right. A half-slice of the microgels is shown in order to better visualise the presence of the cavity. (b) Radial density profiles $\rho(r)$ at the same temperatures with the corresponding colour coding used consistently throughout this work. Together with the numerical data (symbols), fits (lines) are also reported using a Gaussian function (Eq. 11) in the presence of the cavity and using the fuzzy sphere model when this is filled up ($\alpha = 0.8$).

thus separately monitor the behaviour of the radius of gyration and of the hydrodynamic radius as a function of effective temperature, both reported in Figure 4, where one can observe a peculiar feature of hollow microgels. Indeed, R_g is found to display a discontinuity at $\alpha \approx \alpha_{\text{fill}}$ since at this point the structure completely changes its topology. This is reflected in the discontinuous behaviour of the density profiles, reported for values of α from just below to just above α_{fill} in the inset of Fig. 4 (b). Of course, the non-hollow microgel does not exhibit such a feature, showing a much less pronounced swelling. Indeed, for larger values of α , the two curves remain significantly distinct between hollow and non-hollow microgels, with the latter being consistently larger than the hollow case. On the other hand, focusing on the evolution of R_H , we find a rather similar swelling curve for both types of microgels at all temperatures and the absence of a discontinuity for the hollow case. Here, the filling of the cavity is smoothly adsorbed in the variation of the total size. These results are in agreement with experimental Dynamical Light Scattering (DLS) measurements for hollow microgels which have reported a continuous variation for R_H as a function temperature^{18,20,25}. To date, experimental measurements of the variation of R_g , for example by static light scattering, have not yet been reported to our knowledge for hollow microgels.

3.2 How hollow is a hollow microgel?

Having established the main characteristic features of a representative case study of a hollow microgel, we now try to answer numerically this very important question, already asked experimentally some years ago by Dubbert and coworkers¹⁸. To this end, we vary several parameters in the assembly of the microgels to adjust the balance between shell stiffness and thermoresponsiveness. Namely, we perform a large number of simulations changing the shell thickness and the crosslinker concentration. While the former parameter can be modified in experiments by using different sizes for the initial sacrificial core, the latter is the standard control parameter to tune the microgel's softness^{18,25,27}.

We thus initially fix the relative shell thickness to a rather small value, $\delta_{\text{rel}} = 0.21$, and vary the fraction of crosslinkers from 1% to 10%. The corresponding density profiles are reported in Fig. 5 from $\alpha = 0$ to $\alpha = 0.6$ for three values of the crosslinker concentration. We find that for $c = 1\%$ the shell is not able to sustain itself, resulting in a structure that contains monomers within the cavity already at $\alpha = 0.0$. Instead, microgels with $c = 5\%$ and $c = 10\%$ can retain their cavity, at least up to the VPT, even with such a thin shell. As expected, the microgel with a higher crosslinker percentage is stiffer. It is now interesting to ask whether the filling of the cavity still occurs, or if the enhanced stiffness can retard it to the collapsed region or even to completely avoid it. This is a very important question from an application standpoint, as the microgels could preserve their hollowness throughout the volume phase transition. Hence, for the same microgels of Fig. 5, we report the radius of gyration as a function of temperature in Fig. 6 (a). Only for $c = 10\%$ can we detect a discontinuity in correspondence with the cavity filling. Instead, such a discontinuity is not visible for $c = 5\%$, not because the cavity remains intact,

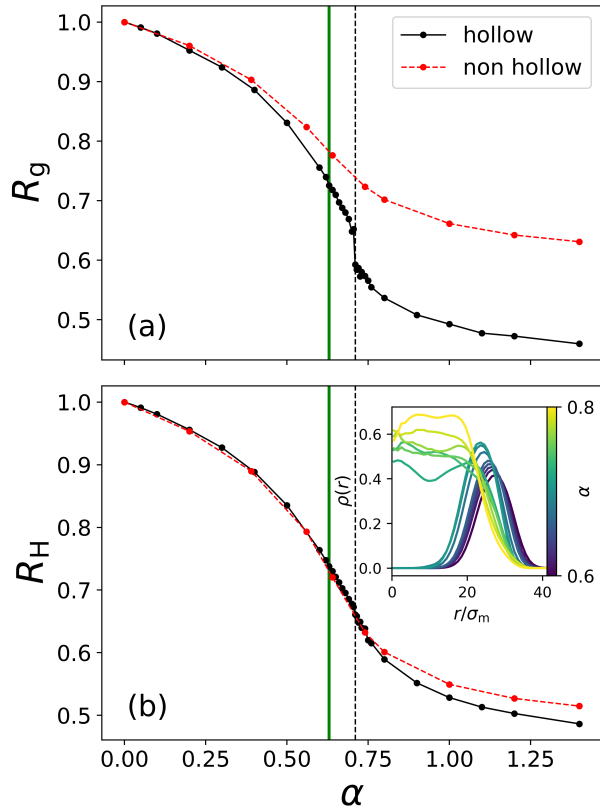


Fig. 4 Swelling curves of the hollow microgel from Figure 3 as well as of a non-hollow microgel of comparable size: (a) radius of gyration and (b) hydrodynamic radius versus effective temperature α . Lines between symbols are guides to the eye. The vertical full line (green) marks the approximate location of the VPT α_{VPT} , while the vertical dashed line (black) represents the point of cavity loss of the hollow microgel α_{fill} . The inset plot in (b) shows many different density profiles of the hollow microgel at different temperatures ($\alpha = 0.6, 0.62, 0.63, 0.64, 0.65, 0.68, 0.7, 0.705, 0.71, 0.715, 0.72, 0.73, 0.75, 0.8$). At $\alpha = 0.705$ we still measure a clear hollow structure and at $\alpha = 0.71$ the microgel's monomers fill the cavity and the microgel changes shape.

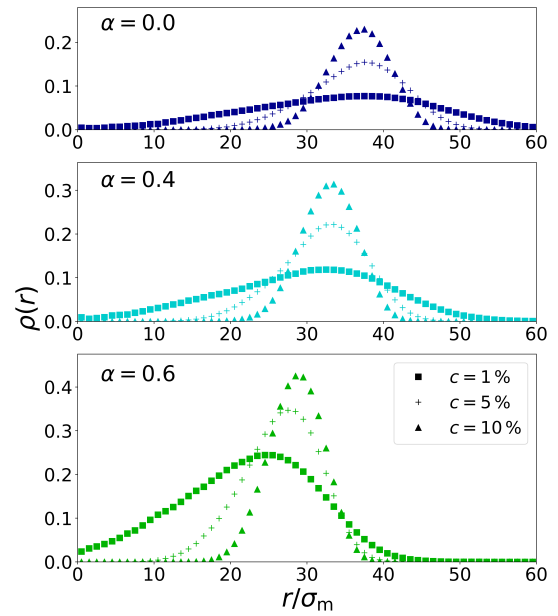


Fig. 5 Radial density distributions for microgels with different crosslinker concentrations c at different temperatures (see labels). The considered microgels have the same relative shell thickness $\delta_{\text{rel}} = 0.21$ and number of monomers $N_m \approx 41000$ (initial boundaries: $Z_{\text{in}} = 50\sigma_m$ and $Z_{\text{out}} = 63\sigma_m$).

but because this happens more or less in correspondence with the VPT and the simultaneous thermal deswelling does not allow for distinction of the filling event. So, it seems that for small shell thickness, even with enhanced stiffness implemented via the presence of the crosslinkers, thermoresponsiveness wins over elasticity, thereby closing the hole and making the microgel non-hollow for temperatures close to or just above the VPT temperature.

We then turn to analyse the opposite case of a much larger relative thickness $\delta_{\text{rel}} = 0.50$, for the same values of crosslinker concentrations. The corresponding swelling curves are also reported in Fig. 6 (a). For these thick hollow microgels, we find that for both $c = 5\%$ and $c = 10\%$, the cavity filling happens at significantly higher values of α compared to smaller shells, and no discontinuity in R_g is detected. In addition, the relative swelling is much more reduced compared to the case of a smaller thickness, even after filling has occurred. Interestingly, for $c = 1\%$, the microgel is now also able to maintain a cavity up to the VPT. However, the softness of the microgel is such that the filling takes place continuously, as shown in the inset of Fig. 6 (a). This demonstrates that shell thickness is a control parameter that can be used alternatively to crosslinker concentration to tune the softness of the hollow microgels. Indeed, increasing δ_{rel} keeping the same c has a similar effect as increasing c at fixed δ_{rel} on the swelling process by moving α_{fill} to higher values. Our findings are in qualitative agreement with available experimental works. In particular, Contreras-Cáceres et al. observed that an increased stiffness, realised through a higher crosslinker percentage, reduces the microgel's thermoresponsiveness²⁵. The same has been discovered by Dubbert et al.¹⁸, who additionally found that an increase in shell thickness also causes the microgel to become less sensitive to temperature. However, it is important to note that the VPT al-

ways happens at around $\alpha \approx 0.63$, where the swelling curves start to change their slope, as shown in Figure 4, thus being unaffected by changing the microgel parameters and therefore unrelated to the cavity loss. The location of α_{fill} with respect α_{VPT} is important in determining how the former manifests in the swelling curves. If α_{fill} is just larger than the VPT value, it will be possible to observe a clear discontinuity in $R_g(\alpha)$ (such as for $c = 10\%$, small thickness in Fig. 7), otherwise if α_{fill} is smaller or comparable to α_{VPT} , there will be no visible sign in the swelling curve ($c = 5\%$ in Fig. 6 (a)). Finally, if the cavity loss happens for temperatures well above the VPT, as for the cases with thicker shells in Figure 6 (a), $R_g(\alpha)$ displays a tiny bump related to α_{fill} . However, it is interesting to focus on this case because it pertains to the stiffest microgel examined in the present work with a high value of $c = 10\%$ and relative thickness $\delta_{\text{rel}} = 0.5$. It has been reported previously that hollow microgels, upon increasing osmotic pressure from added polymer chains, display a fascinating buckling transition. Here, of course, we are examining a microgel on its own but it is legitimate to ask whether the competition between elasticity of the shell and thermoresponsiveness could play a role in modifying the microgel structure. We thus examine the most rigid case in more detail close to the occurrence of the bump, where R_g actually increases again with α , signaling some kind of modification. The corresponding snapshot of the microgel at $\alpha = 1.2$ is reported in Fig. 6 (b,c) and shows a microgel that has completely lost its sphericity adopting a quasi-2D oblate shape. A microgel with the same c but a smaller δ_{rel} instead takes on a bowl-like shape just above the filling, as shown in Fig. 6 (d,e), appearing very close to a buckling transition before it eventually collapses into a small sphere for higher values of α . It will thus be interesting in the future to deepen the investigation of these microgels under crowding conditions, either by adding polymer chains as in Ref.²² or by increasing microgel concentration.

To complete this analysis, it is necessary to quantify the impact of the microgel size. Indeed, simulations are based on coarse-grained monomer modeling, which implies much smaller microgels than in usual experiments. Therefore, we try to assess how α_{fill} is affected by increasing the number of monomers N_m in the microgel representation. This is shown in Fig. 7 (a) where the detected cavity filling is reported for many different microgels. Since N_m can be the same for two microgels with different δ_{rel} and c , we plot α_{fill} vs Z_{out} . It is immediately evident that for increasing N_m the cavity fills at higher and higher values of effective temperature. There does not seem to be a saturation with N_m , particularly for the reference case $\delta_{\text{rel}} = 0.275$ and $c = 5\%$, that is studied up to very large N_m . This result is in agreement with experimental studies of very large hollow microgels, which are found to maintain the cavity open even well above the VPT²⁰ or even to almost lose thermoresponsiveness completely²².

To better visualize the dependence of cavity filling on the shell thickness, we report α_{fill} as a function of δ_{rel} in Fig. 7 (b). We show results for different crosslinker concentrations. An increase in shell thickness, thus in microgel elasticity, has the clear effect of stabilising the hole up to very high temperatures. The opposite is true upon decreasing crosslinker concentration. Importantly, we find that at high enough $\delta_{\text{rel}} = 0.275$ also $c = 1\%$ microgels can

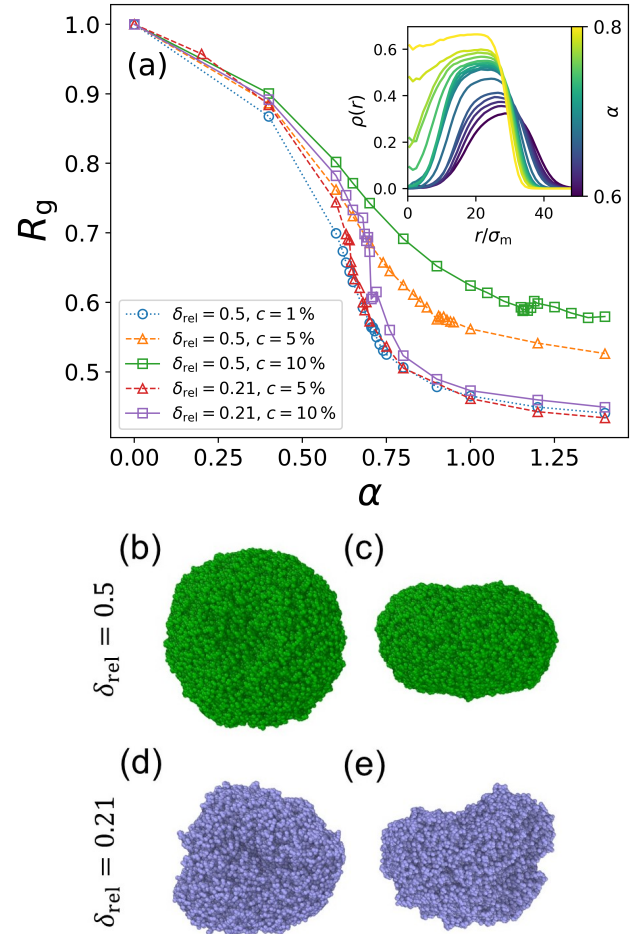


Fig. 6 (a) Swelling curves of different microgels in terms of R_g . All the microgels have the same initial outer assembly border $Z_{\text{out}} = 63 \sigma_m$ while they differ in shell thickness δ_{rel} and crosslinker concentration c . As in Figure 4, the symbols denote all the measured points and the lines serve as a guide for the eye. The thick shells fill their cavity at $\alpha = 0.91$ for $c = 5\%$ and $\alpha = 1.155$ for $c = 10\%$, where a small bump is detected in R_g , while the thin shells fill up significantly earlier at $\alpha = 0.645$ for $c = 5\%$ and $\alpha = 0.705$ for higher crosslinker concentration $c = 10\%$. The inset plot shows the different $\rho(r)$ across α for the $\delta_{\text{rel}} = 0.5$ and $c = 1\%$ case which eventually fills its cavity at $\alpha_{\text{fill}} = 0.72$. Top (b,d) and side (c,e) view of snapshots of a microgel with $\delta_{\text{rel}} = 0.5$ and $c = 10\%$ at $\alpha = 1.2$ and with $\delta_{\text{rel}} = 0.21$, $c = 10\%$ at $\alpha = 0.8$, respectively.

be stabilized as hollow ones up to temperatures around the VPT, something not yet explored in experiments. Hence, these results suggest that an accurate balance between δ_{rel} and c allows one to tune the hollowness of the microgel to the desired temperature, according to the needs of applications.

3.3 Minimum size of a hollow microgel

We already discussed in the previous subsection that the use of a large number of monomers helps to stabilise the cavity. It is now important to ask the opposite question, namely how small a microgel can be while maintaining its cavity. Indeed, the stability of the cavity is an important challenge in establishing a minimal number of monomers to be used for example in computationally feasible bulk simulations. For simplicity, we focus on our reference case $\delta_{\text{rel}} = 0.275$ and $c = 5\%$ and vary N_m in order to establish the lowest number of monomers necessary to observe a clear cavity.

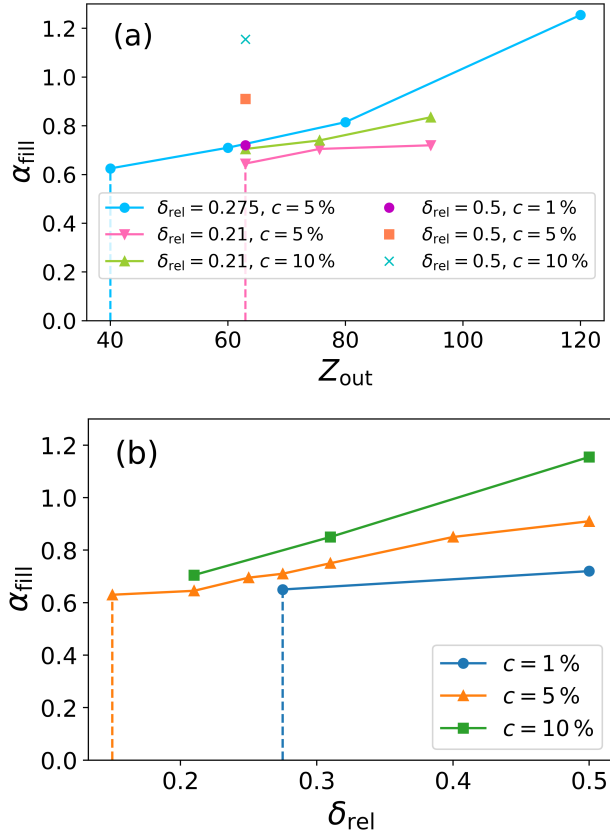


Fig. 7 Cavity loss point α_{fill} for various hollow microgels of different sizes, shown as a function of initial outer radius Z_{out} in (a) and of shell thickness δ_{rel} in (b). Symbols refer to measured data points; solid lines connect microgels with the same crosslinker concentration c . All α_{fill} points are estimated with an accuracy of 0.005 in α . The dashed vertical lines mark the approximate limit for the corresponding parameter (Z_{out} or δ_{rel}) below which it becomes impossible, using the same colour-coded crosslinker percentage, to simulate a hollow microgel that does not show monomers inside the cavity at $\alpha = 0$.

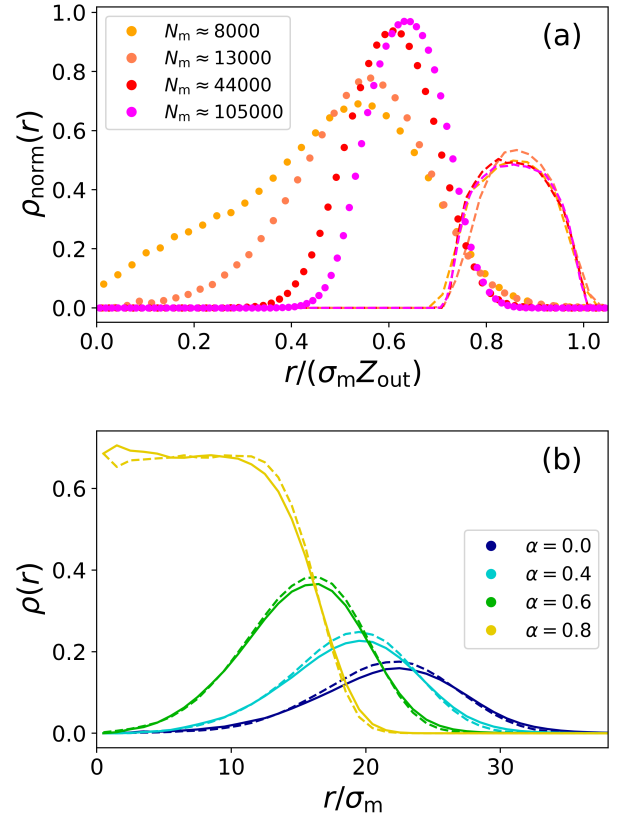


Fig. 8 (a) Normalized density profiles of four different microgels with the same $\delta_{\text{rel}} = 0.275$ and $c = 5\%$ and different size N_m . From left to right, they correspond to: $Z_{\text{out}} = 34.5 \sigma_m, 40 \sigma_m, 60 \sigma_m, 80 \sigma_m$. The dotted lines are the equilibrated profiles at $\alpha = 0$, while the dashed lines represent the initial assembly configuration, resulting from oxDNA. To better visualise the shift with size, data have been x -scaled to the corresponding Z_{out} and y -scaled to a unit integral; (b) density profiles of a $N_m \sim 13000$ microgel with and without the presence of a core in the assembly, as illustrated in Fig. 1 (a) and (b), respectively. Different temperatures are reported: the dashed lines represent the results of the conventional assembly method while the solid lines refer to the core procedure.

Figure 8 (a) shows the normalized density profiles $\rho_{\text{norm}}(r)$ equi-

librated at $\alpha = 0$ (dots) of representative microgels with N_m ranging from ~ 8000 to ~ 105000 . It is immediately evident that the smallest microgel is not hollow, while the cavity becomes more and more pronounced as N_m increases. This can be appreciated best by comparing the density profiles, where the microgel is fully equilibrated in good solvent, with the initial configurations resulting from the assembly (dashed lines). The data have all been scaled to relative distances in order to highlight how the change in shape caused by equilibration depends on microgel size. Hence, for very large N_m , we observe a slight shift of the network distribution closer to the microgel's center of mass, while still preserving a symmetric, almost Gaussian, density profile with a relative thickness very similar to the nominal one from the assembly. As N_m decreases, $\rho(r)$ is found to shift more and more to the center away from the (fixed) initial density profile until it becomes slightly asymmetric for $N_m \sim 13000$ and finally loses the cavity completely below this threshold number of monomers. Incidentally, despite seeming just barely able to sustain the cavity, the profiles for $N_m \sim 13000$ have just enough elasticity to keep the hollowness up to the VPT, as visible from the α -dependence of the density profiles reported in Fig. 8 (b). This is due to the fact that, in general, the enhanced stiffness that the microgel gains by increasing temperature helps to stabilize the cavity, even very close to the threshold of stability. Therefore, the present investigation suggests that for the chosen values of $\delta_{\text{rel}} = 0.275$ and $c = 5\%$, we need at least $N_m \sim 13000$ to be able to simulate truly hollow microgels. However, to assess whether we may further reduce N_m to speed up simulations, we also attempt a different assembly process in the presence of a physical core, as described in Methods and illustrated in Fig. 1 (b). The corresponding results, also shown in Fig. 8 (b), indicate no major differences between the radial density distributions obtained with both methods. The small systematic deviations between the two curves do not exceed the differences obtained from different assembly runs. Hence, despite assembly under different conditions, the final structure of the network is solely determined by the stiffness of the shell. Of course, more refined assemblies could be used, for example by bonding the shell to the physical core with patches that might increase nucleation in that region to increase monomer density close to the core. However, for very small microgels, we expect that this approach will not make a major difference. Therefore, we conclude that we can stick to our simpler assembly protocol in the absence of the core, and for each set of parameters, δ_{rel} and c , we need to adjust the minimum number of monomers needed to reliably obtain hollow structures. This number is of the order of 10^4 monomers, which is a low enough number to allow for multiple microgel simulations within present computational resources¹³.

3.4 Form factor analysis and comparison to experiments.

In this last section, we focus on reporting the form factors $P(q)$, directly calculated from our simulations, for different hollow microgels. We describe them with the models explained in the Methods section. We then try to compare some numerical predictions with available experimental data.

We show $P(q)$ for hollow microgels with $c = 5\%$ and two dif-

ferent relative thicknesses in Fig. 9. In particular, data refer to relatively thin microgels ($\delta_{\text{rel}} = 0.275$) in panel (a) and to thicker shells in panel (b). We use two approaches to describe the data: (i) we fit the corresponding density profiles, then evaluate the Fourier transform with the obtained fit parameters and (ii) we directly fit the form factors and compare the resulting fit parameters to the previous ones. The two approaches turn out to be indistinguishable from each other, confirming the robustness of the results. We find that the simple Gaussian form factors capture the behaviour of the thinner microgels reported in Eq. 12 quite well, while the parabolic model with $W = 0$, as explained in the Methods, describes them with equal precision. This is true as long as the cavity stays open, for $\alpha \lesssim \alpha_{\text{fill}}$, but for higher temperatures it is necessary to use the fuzzy sphere model. The change in topology for $P(q)$ is clearly evident in Fig. 9 (a) for $\alpha = 0.8$ compared to the other temperatures since it displays less sharp minima that indicate a 'fuzzy-sphere-like' structure. Next, we examine thicker hollow microgels in Fig. 9 (b), where the Gaussian shape of the density profiles no longer holds. To describe the form factor of the thicker microgel with $\delta_{\text{rel}} = 0.5$, we then resort to the parabolic approach with $W \neq 0$ for both the density profiles and the form factors (Eq. 8 and 10). This procedure is now applied to all α reported, because this microgel maintains its hollow character even at $\alpha = 0.8$.

We summarize all the fit parameters for the two sets of microgels at the different values of α , illustrated in Fig. 9, in Table 1. Parameters are listed both resulting from density profiles and from form factor fits, confirming that the two methods yield very similar results. Similarly, a consistency is obtained between Gaussian and parabolic (with $W = 0$) functional forms for the thinner microgels. Of course, for small enough microgels, the Gaussian approach can be preferred, especially for describing numerical data, due to the smaller number of fit parameters involved.

We can now directly compare the simulation results to experimental candidates. We start by examining the experiments of Hazra and coworkers²⁰ since these hollow microgels have a shell thickness and crosslinker percentage close to our reference case ($\delta_{\text{rel}} = 0.275$ and $c \approx 5\%$). The experimental form factors of these rather large microgels, measuring approximately $1\mu\text{m}$ in the swollen state, have been measured by static light scattering at two different temperatures, 20°C and 40°C . The comparison between experimental and numerical form factors at these two temperatures is reported in Fig. 10 (a), where the numerical curves have been shifted on q -axis by a common factor for each temperature, identifying the value of σ_m that is used in the coarse-graining approach (see caption of Figure 10 (a)). After rescaling the position of the first peak, we find that the subsequent peaks also match the positions of the experimental form factors, especially for the largest simulated microgel ($N_m \approx 355000$), allowing us to identify that $\alpha = 0.0$ corresponds to $T = 20^\circ\text{C}$, while $\alpha = 0.65$ is consistent with $T = 40^\circ\text{C}$. The comparison confirms that the numerical model is able to well describe the experimental behaviour and, most importantly, to reproduce the presence of the cavity for both temperatures²⁰.

As an additional test, we then compare our simulations to much smaller microgels, measured by Small Angle Neutron Scattering

Table 1 Full set of parameters obtained from fitting $\rho(r)$ (with an added index ρ) or $P(q)$ (same symbols without index) using a parabolic fit with $W > 0$ for the density profile (Eq. 8) of the microgel with $\delta_{rel} = 0.50$ ($Z_{in} = 31.5\sigma_m$ and $Z_{out} = 63\sigma_m$), while using both a Gaussian (Eq. 11) and a parabolic fit with $W = 0$ (Eq. 8) for $\delta_{rel} = 0.275$ ($Z_{in} = 43.5\sigma_m$ and $Z_{out} = 60\sigma_m$) up to $\alpha = 0.6$. Lengths are given in units of σ_m .

| $\delta_{rel} = 0.50, N_m \approx 73000$ ($Z_{in} = 31.5\sigma_m$ and $Z_{out} = 63\sigma_m$ (Eq. 8 with $W \neq 0$)) | | | | | | | | | | |
|---|-----------------|-----------------|------------------|------------------|------------------|------------------|-----------------|------------------|-----------------|-----------------|
| α | $s_{in,\rho}$ | s_{in} | $s_{out,\rho}$ | s_{out} | $R_{out,\rho}$ | R_{out} | W_ρ | W | a_ρ | a |
| 0.0 | 8.27 ± 0.07 | 8.10 ± 5.28 | 7.37 ± 0.07 | 9.40 ± 2.24 | 46.58 ± 0.02 | 46.07 ± 1.09 | 6.45 ± 0.12 | 3.70 ± 9.62 | 0.20 ± 0.00 | 0.23 ± 0.03 |
| 0.4 | 7.49 ± 0.06 | 8.60 ± 4.43 | 6.61 ± 0.06 | 8.57 ± 4.43 | 41.33 ± 0.02 | 40.73 ± 1.10 | 5.53 ± 0.11 | 1.29 ± 8.74 | 0.29 ± 0.00 | 0.33 ± 0.04 |
| 0.6 | 6.35 ± 0.04 | 6.78 ± 3.54 | 5.72 ± 0.04 | 6.38 ± 1.52 | 35.71 ± 0.01 | 35.59 ± 0.65 | 5.26 ± 0.07 | 3.89 ± 6.32 | 0.44 ± 0.00 | 0.47 ± 0.04 |
| 0.8 | 4.78 ± 0.02 | 4.15 ± 5.33 | 4.19 ± 0.02 | 3.41 ± 1.52 | 29.96 ± 0.02 | 30.15 ± 0.35 | 8.44 ± 0.03 | 10.21 ± 7.23 | 0.69 ± 0.00 | 0.71 ± 0.03 |
| $\delta_{rel} = 0.275, N_m \approx 44000$, ($Z_{in} = 43.5\sigma_m$ and $Z_{out} = 60\sigma_m$ (Eq. 8 with $W = 0$ and Eq. 11)) | | | | | | | | | | |
| α | $s_{in,\rho}$ | s_{in} | $s_{out,\rho}$ | s_{out} | $R_{out,\rho}$ | R_{out} | a_ρ | a | | |
| 0.0 | 7.21 ± 0.08 | 5.94 ± 1.76 | 6.37 ± 0.07 | 8.23 ± 1.33 | 43.25 ± 0.03 | 43.25 ± 0.43 | 0.29 ± 0.00 | 0.21 ± 0.01 | | |
| 0.4 | 6.51 ± 0.07 | 6.12 ± 1.37 | 5.97 ± 0.07 | 6.91 ± 1.07 | 38.32 ± 0.03 | 38.52 ± 0.31 | 0.27 ± 0.00 | 0.28 ± 0.01 | | |
| 0.6 | 5.82 ± 0.05 | 5.24 ± 1.13 | 5.41 ± 0.05 | 6.47 ± 0.85 | 32.92 ± 0.02 | 33.02 ± 0.27 | 0.41 ± 0.00 | 0.42 ± 0.01 | | |
| α | σ_ρ | σ | μ_ρ | μ | C_ρ | C | | | | |
| 0.0 | 5.40 ± 0.02 | 5.14 ± 0.08 | 36.35 ± 0.02 | 36.31 ± 0.04 | 0.20 ± 0.00 | 0.23 ± 0.00 | | | | |
| 0.4 | 4.87 ± 0.01 | 4.66 ± 0.06 | 32.10 ± 0.01 | 32.05 ± 0.03 | 0.28 ± 0.00 | 0.31 ± 0.00 | | | | |
| 0.6 | 4.38 ± 0.01 | 4.22 ± 0.05 | 27.31 ± 0.02 | 27.24 ± 0.03 | 0.43 ± 0.00 | 0.46 ± 0.00 | | | | |

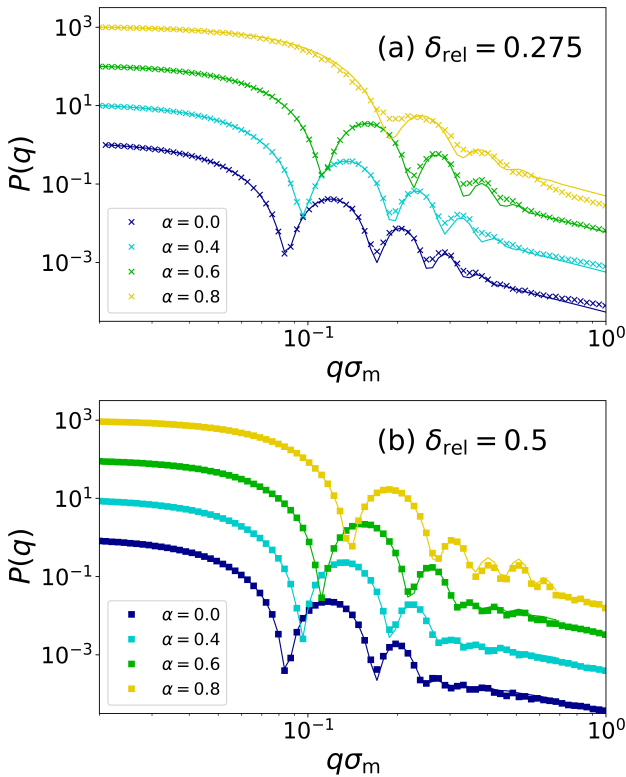


Fig. 9 Form factors $P(q)$ for microgels with $c=5\%$ and (a) $\delta_{rel} = 0.275$ and (b) $\delta_{rel} = 0.5$ for different values of α , arbitrarily shifted vertically to improve visualization. Symbols are numerical data and lines are fits obtained using the Gaussian approximation in equation 12 for the curves in (a) with $\alpha = 0-0.6$, the fuzzy sphere model for $\alpha = 0.8$, and finally the parabolic approach in (b) for all α .

by Dubbert and coworkers in Ref. ¹⁸. In this regard, we consider microgels with a shell thickness of $\delta_{rel} = 0.5$ and $c \approx 5\%$, and perform the fits of the experimental data with SasView⁴³ using a hollow functional form plus a Lorentzian, as reported in the original paper. We remark that these fits yield density profiles similar to the ones of Ref. ¹⁸, resulting in a rather asymmetric shell at low T and a slightly hollow structure at high T (see Fig. 8, c2-d2 of the original paper). Having performed the fits, we can then exclude the resolution (also taken to be the same as reported in the paper) and the polydispersity from the data, in order to better compare with the simulations. We find that the data are again reasonably well described by our simulations, particularly in the position of the multiple peaks at high T . Some small deviations are to be expected by the errors introduced by the fits, the reduced size of the numerical microgels, and the uncertainty in δ_{rel} . Notwithstanding these, we find a similar α - T relationship as for the previous comparison, giving us further confidence in the employed numerical model. Finally and most importantly, both experiments and simulations show how large enough microgels with thick shells possess enough elasticity to prevent cavity loss at high T .

4 Discussion and Conclusions

In this work, we took advantage of computer simulations of a realistic microgel model to investigate in detail the swelling behaviour of hollow microgels with different characteristics across the Volume Phase Transition. In an attempt to quantify the effects of softness and thermoresponsiveness on the hollowness of the microgel and on how this can persist even beyond the VPT, we varied the main control parameters that are used in experiments. In particular, we tuned the crosslinker concentration and the relative shell thickness to modulate the filling of the cavity in relation to the occurrence of the VPT. While the latter is fixed by the polymer affinity to the solvent to always occur at the same temperature, the former can thus be experimentally adjusted. Our simulations found that the filling manifests itself, under appropriate conditions, as a discontinuous behaviour of the radius of gyration as a function of temperature. In particular, we found that increasing the crosslinker concentration has qualitatively a similar effect to increasing the shell thickness. However, while c acts at a lo-

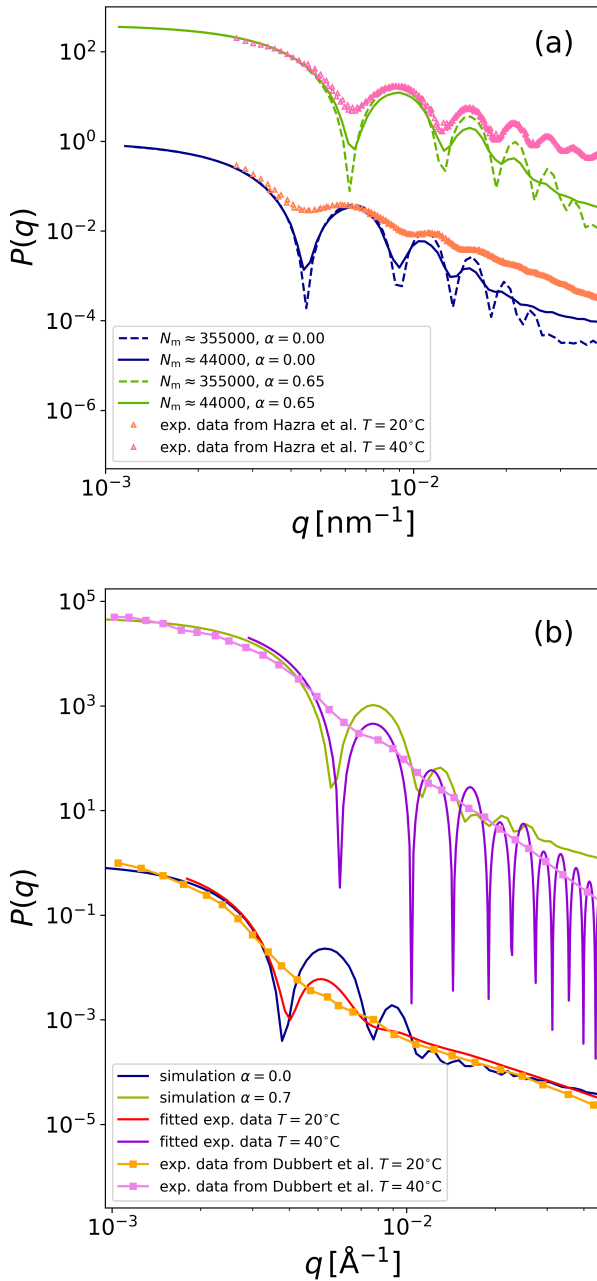


Fig. 10 Comparison of numerical (lines) and experimental form factors (symbols). The latter are taken from (a) Ref.²⁰ for hollow microgels with $\delta_{\text{rel}} \sim 0.275$ and $c \sim 5\%$. The simulation curves have been rescaled not only on the y-axis but also on the x-axis using the factor $q_{\text{exp}} = q_{\text{sim}}/\sigma_m$ with $\sigma_m \approx 19.3\text{ nm}$ for the smaller microgel ($Z_{\text{in}} = 60\sigma_m$ and $Z_{\text{out}} = 43.5\sigma_m$) and $\sigma_m \approx 8.9\text{ nm}$ for the biggest one studied here: $Z_{\text{in}} = 87\sigma_m$ and $Z_{\text{out}} = 120\sigma_m$. Data have been shifted vertically to improve visualisation; (b) and from Ref.¹⁸ for hollow microgels with $\delta_{\text{rel}} \sim 0.5$ and $c \sim 5\%$. We extracted the form factors of sample PP2 from Ref.¹⁸ and then performed the fits via SasView⁴³ to remove polydispersity and resolution in order to better compare with simulations. The simulated data ($Z_{\text{out}} = 63\sigma_m$, $Z_{\text{in}} = 31.5\sigma_m$) have been shifted on the q -axis as in (a) by $\sigma_m \approx 2.2\text{ nm}$.

cal level defining the overall stiffness of the shell, δ_{rel} dictates the topology of the microgel. Thus, a larger shell thickness provides an increase in the value of W in Eq. 8, yielding a microgel with a different structure than for thin shells, where $W = 0$, indicating a transition from parabolic to Gaussian density profiled. This qualitative change also impacts the swelling process, making a sharp discontinuity in $R_g(\alpha)$ much more likely for thinner shells (see inset of Fig. 6 (a)). Therefore, such a discontinuity should be looked for in experiments by focusing on microgels with thin shells and a high enough crosslinker percentage, allowing them to maintain the cavity just above the VPTT. Importantly, we do not observe a similar feature in the swelling behavior of the hydrodynamic radius, due to the stronger influence of the outer chains on this quantity and possibly also to the reduced numerical system size, which may disfavor the observation of a discontinuity in the total microgel size. Indeed, experimental measurements of R_H have not detected such a behavior so far, but it may be worth searching for it by directly measuring R_g .

In order to assess the importance of size effects in our study, we prepared microgels of different sizes and numbers of monomers N_m ranging between 10^4 and 10^5 . We then reported several of the microgel properties as a function of N_m , finding that increasing the size enhances the stiffness of the shell with respect to cavity filling. However, we also determined $\sim 10^4$ as the lower limit of stability of hollow microgels for realistic numerical modelling in future studies. Indeed, once prepared with a nominal cavity, all initial confinements are removed, as in experiments by the dissolution of the core, the shell tends to partially fill the hole, as also seen experimentally by Dubbert et al.¹⁸ who monitored the structure of the microgels before and after core dissolution. These experimental data have been directly compared to our numerical model in terms of form factors for different temperatures, finding satisfactory agreement. A similar correspondence between experiments and simulations has been found also for much larger microgels, more recently synthesized by Hazra and coworkers²⁰. In addition, the dependence of the cavity filling temperature α_{fill} on the crosslinker concentration or shell thickness was found to be in qualitative agreement with available experiments^{18,25}. These results give us confidence in the numerical model, opening the way to extend our analysis to the collective behaviour of hollow microgels under crowded conditions. A first study in this direction was put forward in Ref.⁴⁴ where the behaviour of hollow microgels was studied in a binary mixture of hollow and regular microgels, revealing through simulations that for the studied parameters hollow microgels experience an effective potential that is softer than for regular ones. Another interesting direction to pursue in the future is to assess the role of charges on the swelling response of hollow microgels, as initially done by Hazra and coworkers²⁰. However, it is already known that the presence of ionic groups favours the stretching of the network³⁹ and thus should effectively act as an additional contribution to the stiffness of the network. Their presence could thus modify the response to external stimuli such as pH, which could hold promises for practical purposes.

Finally, the present study suggests that different behaviours are observed when the elasticity of microgels is enhanced. For exam-

ple, the microgels have a stronger tendency to deform, as in the case of $c = 10\%$ (see snapshots of Fig. 7). Such interesting properties may thus be enhanced by the presence of charged groups within the shell. We also explored the very soft case of hollow microgels with $c = 1\%$, which was found to be able to sustain its cavity up to the VPT for a large enough shell thickness. This avenue could be further explored in experiments, where mostly microgels with $c \geq 5\%$ have been considered so far. In summary, our work can provide useful guidelines for both experiments and simulations in selecting the best parameters in the synthesis of the microgels to enhance or tune their hollowness at a desired temperature and to optimize their use for specific applications.

Author Contributions

Author contributions are defined based on CRediT (Contributor Roles Taxonomy). Conceptualization: E.Z.; Formal analysis: L.R.,E.Z.; Funding acquisition: E.Z.; Investigation: L.R.,E.Z.; Methodology: L.R.,E.Z.; Project administration: E.Z.; Supervision: E.Z.; Validation: L.R.,E.Z.; Visualization: L.R.; Writing – original draft: L.R.,E.Z.; Writing – review and editing: L.R.,E.Z..

Conflicts of interest

There are no conflicts to declare.

Data availability

Data for this article will be made available via ZENODO.

Appendix

Fourier transformation of parabolic density distribution

Since for the parabolic approximation of the density profile, $\rho_{\text{parab}}(r)$ is made up of $i = 4$ consecutive parabolas (cf. equ. 8) which we call here $\rho_i(r)$, the full amplitude $A_{\text{parab}}(q)$ contains four terms:

$$\begin{aligned}
 A_1(q) &= 4\pi \int_{R_{\text{in}}-s_{\text{in}}}^{R_{\text{in}}} \rho_1(r) \frac{\sin qr}{qr} r^2 dr \\
 &= \frac{1}{2q^5 s_{\text{in}}^2} a \left((-q^3 R_{\text{in}} s_{\text{in}}^2 + 2q(R_{\text{in}} + 2s_{\text{in}})) \cos(qR_{\text{in}}) \right. \\
 &\quad \left. - 2q(R_{\text{in}} - s_{\text{in}}) \cos(q(R_{\text{in}} - s_{\text{in}})) - 6 \sin(qR_{\text{in}}) \right. \\
 &\quad \left. + 2q^2 R_{\text{in}} s_{\text{in}} \sin(qR_{\text{in}}) + q^2 s_{\text{in}}^2 \sin(qR_{\text{in}}) \right. \\
 &\quad \left. + 6 \sin(q(R_{\text{in}} - s_{\text{in}})) \right), \tag{13}
 \end{aligned}$$

$$\begin{aligned}
 A_2(q) &= 4\pi \int_{R_{\text{in}}}^{R_{\text{in}}+s_{\text{in}}} \rho_2(r) \frac{\sin qr}{qr} r^2 dr \\
 &= \frac{1}{2q^5 s_{\text{in}}^2} a \left(q(-4s_{\text{in}} + R_{\text{in}}(2 + q^2 s_{\text{in}}^2)) \cos(qR_{\text{in}}) \right. \\
 &\quad \left. - 2q(R_{\text{in}} + s_{\text{in}})(1 + q^2 s_{\text{in}}^2) \cos(q(R_{\text{in}} + s_{\text{in}})) \right. \\
 &\quad \left. - (6 + q^2 s_{\text{in}}(2R_{\text{in}} + s_{\text{in}})) \sin(qR_{\text{in}}) \right. \\
 &\quad \left. + 2(3 + q^2 s_{\text{in}}^2) \sin(q(R_{\text{in}} + s_{\text{in}})) \right), \tag{14}
 \end{aligned}$$

$$\begin{aligned}
 A_3(q) &= 4\pi \int_{R_{\text{out}}-s_{\text{out}}}^{R_{\text{out}}} \rho_3(r) \frac{\sin qr}{qr} r^2 dr \\
 &= -\frac{1}{2q^5 s_{\text{out}}^2} a \left(q(4s_{\text{out}} + R_{\text{out}}(2 + q^2 s_{\text{out}}^2)) \cos(qR_{\text{out}}) \right. \\
 &\quad \left. - 2q(R_{\text{out}} - s_{\text{out}})(1 + q^2 s_{\text{out}}^2) \cos(q(R_{\text{out}} - s_{\text{out}})) \right. \\
 &\quad \left. - 6 \sin(qR_{\text{out}}) + 2q^2 R_{\text{out}} s_{\text{out}} \sin(qR_{\text{out}}) \right. \\
 &\quad \left. - q^2 s_{\text{out}}^2 \sin(qR_{\text{out}}) + 6 \sin(q(R_{\text{out}} - s_{\text{out}})) \right. \\
 &\quad \left. + 2q^2 s_{\text{out}}^2 \sin(q(R_{\text{out}} - s_{\text{out}})) \right), \tag{15}
 \end{aligned}$$

$$\begin{aligned}
 A_4(q) &= 4\pi \int_{R_{\text{out}}}^{R_{\text{out}}+s_{\text{out}}} \rho_4(r) \frac{\sin qr}{qr} r^2 dr \\
 &= \frac{1}{2q^5 s_{\text{out}}^2} a \left(q(4s_{\text{out}} + R_{\text{out}}(-2 + q^2 s_{\text{out}}^2)) \cos(qR_{\text{out}}) \right. \\
 &\quad \left. + 2q(R_{\text{out}} + s_{\text{out}}) \cos(q(R_{\text{out}} + s_{\text{out}})) \right. \\
 &\quad \left. + (6 + q^2(2R_{\text{out}} - s_{\text{out}})s_{\text{out}}) \sin(qR_{\text{out}}) \right. \\
 &\quad \left. - 6 \sin(q(R_{\text{out}} + s_{\text{out}})) \right), \tag{16}
 \end{aligned}$$

and in case $W \neq 0$ there is an additional term in between:

$$\begin{aligned}
 A_5(q) &= 4\pi \int_{R_{\text{in}}+s_{\text{in}}}^{R_{\text{out}}-s_{\text{out}}} a \cdot \frac{\sin qr}{qr} r^2 dr \\
 &= \frac{a}{q^3} \left(q(R_{\text{in}} + s_{\text{in}}) \cos(q(R_{\text{in}} + s_{\text{in}})) \right. \\
 &\quad \left. + q(-R_{\text{out}} + s_{\text{out}}) \cos(q(R_{\text{out}} - s_{\text{out}})) \right. \\
 &\quad \left. - \sin(q(R_{\text{in}} + s_{\text{in}})) + \sin(q(R_{\text{out}} - s_{\text{out}})) \right) \tag{17}
 \end{aligned}$$

They can now all be added to make up the total Fourier transformation $A_{\text{parab}}(q) = A_1(q) + A_2(q) + A_3(q) + A_4(q) + (A_5(q))$ which can then be used for equation 10.

Acknowledgements

We thank Jerome Crassous and Walter Richtering for providing the experimental form factors shown in Fig. 10. We also thank Lorenzo Rovigatti and Rodrigo Rivas-Barbosa for help regarding the assembly method in the presence of a core and Yuri Gerelli for help with the SasView fits. We acknowledge financial support from the European Union (HorizonMSCA-Doctoral Networks) through the project QLUSTER (HORIZON-MSCA-2021-DN-01-GA101072964). This work also benefited from the use of the SasView application, originally developed under NSF award DMR-0520547. SasView contains code developed with funding from the European Union's Horizon 2020 research and innovation programme under the SINE2020 project, grant agreement No. 654000.

Notes and references

- 1 R. Pelton and T. Hoare, in *Microgels and Their Synthesis: An Introduction*, John Wiley & Sons, Ltd, 2011, ch. 1, pp. 1–32.
- 2 R. Pelton, *Advances in Colloid and Interface Science*, 2000, **85**, 1–33.
- 3 M. Stieger, W. Richtering, J. Pedersen and P. Lindner, *The Journal of chemical physics*, 2004, **120**, 6197–206.
- 4 R. Pelton and P. Chibante, *Colloids and Surfaces*, 1986, **20**, 247–256.
- 5 T. Hoare and R. Pelton, *Macromolecules*, 2004, **37**, 2544–2550.
- 6 M. Bajomo, J. H. G. Steinke and A. Bismarck, *The Journal of Physical Chemistry B*, 2007, **111**, 8655–8662.
- 7 T. López-León and A. Fernández-Nieves, *Phys. Rev. E*, 2007, **75**, 011801.
- 8 X. Xia, S. Tang, X. Lu and Z. Hu, *Macromolecules*, 2003, **36**.
- 9 I. M. Lifshitz, *Journal of Experimental and Theoretical Physics*, 1969.
- 10 C. Wu and X. Wang, *Phys. Rev. Lett.*, 1998, **80**, 4092–4094.
- 11 L. A. Lyon and A. Fernandez-Nieves, *Annual review of physical chemistry*, 2012, **63**, 25–43.
- 12 P. J. Yunker, K. Chen, M. D. Gratale, M. A. Lohr, T. Still and A. Yodh, *Reports on Progress in Physics*, 2014, **77**, 056601.
- 13 G. Del Monte and E. Zaccarelli, *Physical Review X*, 2024, **14**, 041067.
- 14 L. A. Lyon, G. R. Hendrickson, Z. Meng and A. N. St. John Iyer, in *Exploiting the Optical Properties of Microgels and Hydrogels as Microlenses and Photonic Crystals in Sensing Applications*, John Wiley & Sons, Ltd, 2011, ch. 14, pp. 355–374.
- 15 Y. Ben, I. Robb, P. Tonmukayakul and Q. Wang, in *Microgels for Oil Recovery*, John Wiley & Sons, Ltd, 2011, ch. 16, pp. 407–422.
- 16 E. Pashkovski, in *Applications of Biopolymer Microgels*, John Wiley & Sons, Ltd, 2011, ch. 17, pp. 423–450.
- 17 M. Karg, A. Pich, T. Hellweg, T. Hoare, L. A. Lyon, J. Crassous, D. Suzuki, R. A. Gumerov, S. Schneider, I. I. Potemkin *et al.*, *Langmuir*, 2019, **35**, 6231–6255.
- 18 J. Dubbert, T. Honold, J. Pedersen, A. Radulescu, M. Drechsler, M. Karg and W. Richtering, *Macromolecules*, 2014, **47**, 8700–8708.
- 19 G. Liu, C. Zhu, J. Xu, Y. Xin, T. Yang, J. Li, L. Shi, Z. Guo and W. Liu, *Colloids and Surfaces B: Biointerfaces*, 2013, **111**, 7–14.
- 20 N. Hazra, J. Lammertz, A. Babenyshev, R. Erkes, F. Hagemans, C. Misra, W. Richtering and J. J. Crassous, *Soft Matter*, 2024, **20**, 4608–4620.
- 21 H. Noguchi and G. Gompper, *Proceedings of the National Academy of Sciences*, 2005, **102**, 14159–14164.
- 22 F. Hagemans, F. Camerin, N. Hazra, J. Lammertz, F. Dux, G. Del Monte, O.-V. Laukkanen, J. J. Crassous, E. Zaccarelli and W. Richtering, *ACS Nano*, 2023, **17**, 7257–7271.
- 23 F. m. c. Quemeneur, C. Quilliet, M. Faivre, A. Viallat and B. Pépin-Donat, *Phys. Rev. Lett.*, 2012, **108**, 108303.
- 24 J. L. McWhirter, H. Noguchi and G. Gompper, *Soft Matter*, 2011, **7**, 10967–10977.
- 25 R. Contreras-Cáceres, L. Schellkopf, C. Fernández-López, I. Pastoriza-Santos, J. Pérez-Juste and M. Stamm, *Langmuir*, 2015, **31**, 1142–1149.
- 26 M. F. Schulte, A. Scotti, A. P. Gelissen, W. Richtering and A. Mourran, *Langmuir*, 2018, **34**, 4150–4158.
- 27 K. Geisel, A. A. Rudov, I. I. Potemkin and W. Richtering, *Langmuir*, 2015, **31**, 13145–13154.
- 28 S. Nayak, D. Gan, M. Serpe and L. Lyon, *Small*, 2005, **1**, 416–421.
- 29 J. Vialetto, F. Camerin, F. Grillo, S. N. Ramakrishna, L. Rovigatti, E. Zaccarelli and L. Isa, *ACS Nano*, 2021, **15**, 13105–13117.
- 30 N. Gnan, L. Rovigatti, M. Bergman and E. Zaccarelli, *Macromolecules*, 2017, **50**, 8777–8786.
- 31 P. Šulc, F. Romano, T. E. Ouldridge, L. Rovigatti, J. P. K. Doye and A. A. Louis, *The Journal of Chemical Physics*, 2012, **137**, 135101.
- 32 A. Ninarello, J. J. Crassous, D. Paloli, F. Camerin, N. Gnan, L. Rovigatti, P. Schurtenberger and E. Zaccarelli, *Macromolecules*, 2019, **52**, 7584–7592.
- 33 K. Kremer and G. S. Grest, *Journal of Chemical Physics*, 1990, **92**, 5057–5086.
- 34 T. Soddemann, B. Duenweg and K. Kremer, *European Physical Journal E*, 2001, **6**, 409–419.
- 35 F. Lo Verso, J. A. Pomposo, J. Colmenero and A. J. Moreno, *Soft Matter*, 2015, **11**, 1369–1375.
- 36 S. Nosé, *The Journal of Chemical Physics*, 1984, **81**, 511–519.
- 37 M. Rubinstein and R. H. Colby, *Polymer Physics*, Oxford University Press, 2003, pp. 60–61.
- 38 J. B. Hubbard and J. F. Douglas, *Physical Review E*, 1993, **47**, R2983.
- 39 G. Del Monte, D. Truzzolillo, F. Camerin, A. Ninarello, E. Chauveau, L. Tavagnacco, N. Gnan, L. Rovigatti, S. Senato and E. Zaccarelli, *Proceedings of the National Academy of Sciences*, 2021, **118**, e2109560118.
- 40 I. Berndt, J. S. Pedersen and W. Richtering, *Journal of the American Chemical Society*, 2005, **127**, 9372–9373.
- 41 S. J. Mears, Y. Deng, T. Cosgrove and R. Pelton, *Langmuir*,

- 1997, **13**, 1901–1906.
- 42 M. Gradzielski, D. Langevin, L. Magid and R. Strey, *The Journal of Physical Chemistry*, 1995, **99**, 13232–13238.
- 43 *SasView*, <http://www.sasview.org/>.
- 44 A. V. Petrunin, T. Höfken, S. Schneider, P. Mota-Santiago, J. E. Houston and A. Scotti, *Soft Matter*, 2024, **20**, 8125–8135.